

1

2

Global Biogeochemical Cycles

3

Supporting Information for

4

Update on the Temperature Corrections of Global Air-Sea CO₂ Flux Estimates

5

Yuanxu Dong^{1,2}, Dorothee C. E. Bakker^{1*}, Thomas G. Bell², Boyin Huang³, Peter Landschützer⁴, Peter

6

S. Liss¹, Mingxi Yang²

7

¹Centre for Ocean and Atmospheric Sciences, School of Environmental Sciences, University of East Anglia, Norwich, UK;

8

²Plymouth Marine Laboratory, Prospect Place, Plymouth, UK; ³National Centers for Environmental Information, National

9

Oceanic and Atmospheric Administration, Asheville, NC, USA; ⁴Max Planck Institute for Meteorology, Hamburg, Germany

10

Correspondence to: Yuanxu Dong (Yuanxu.Dong@uea.ac.uk) and Dorothee C. E. Bakker (D.Bakker@uea.ac.uk)

11

Contents of this file

13

14 Text S1 to S5

15 Figures S1 to S4

16 Table S1

17 SI References

18

Additional Supporting Information (Files uploaded separately)

20

21 Dataset S1

22

23

Text S1. Conversion of CO₂ Concentration

25 The mole fraction of the equilibrated CO₂ ($\chi_{\text{CO}_2\text{w}}$) in the equilibrator is measured by a gas analyzer

26 and is then converted into CO₂ partial pressure ($p_{\text{CO}_2\text{w_equ}}$) using the equilibrator temperature (T_{equ} ,

27 K) and pressure (P_{equ} , atm):

28

$$p_{\text{CO}_2\text{w_equ}} = \chi_{\text{CO}_2\text{w}}(P_{\text{equ}} - p_{\text{H}_2\text{O}}) \quad (\text{S1})$$

29 where $p_{\text{H}_2\text{O}}$ (atm) is the water vapor pressure and can be calculated from T_{equ} and the seawater
30 salinity (Pierrot et al., 2009). The $p\text{CO}_{2\text{w_equ}}$ is then converted into $f\text{CO}_{2\text{w_equ}}$ to correct for non-ideal
31 behavior of the gas (Weiss, 1974):

$$32 \quad f\text{CO}_{2\text{w_equ}} = \gamma p\text{CO}_{2\text{w_equ}} \quad (\text{S2})$$

33 where the fugacity coefficient γ is ~ 0.996 (Bakker et al., 2014).

34

35 **Text S2. The Timescale of Chemical Repartitioning and Water Mass Transport**

36 The seawater carbonate system creates unique properties for air-sea CO_2 exchange. The seawater
37 carbonate system includes several different carbonate species, i.e., CO_2 , carbonic acid, bicarbonate,
38 carbonate. Among these species, only CO_2 is directly involved in the air-sea CO_2 exchange. There is
39 a dynamic equilibrium between these carbonate species. When the seawater temperature varies,
40 these carbonate species repartition and gradually approach a new equilibrium. The relaxation time
41 (the time after which a perturbation has reached e^{-1} of its initial value) for this equilibration depends
42 on pH and temperature. For typical seawater (pH ~ 8.2 , total dissolved inorganic carbon $\sim 2000 \mu\text{mol}$
43 kg^{-1} , and salinity ~ 35) at $\sim 25^\circ\text{C}$, the relaxation time is ~ 13 s (Johnson, 1982; Zeebe & Wolf-Gladrow,
44 2001). For warmer seawater (e.g., $\sim 30^\circ\text{C}$), the relaxation time is shorter (~ 11 s) (Johnson, 1982; Zeebe
45 & Wolf-Gladrow, 2001), while for colder seawater, the relaxation time is longer. Therefore, the
46 timescale of the chemical repartitioning of the CO_2 system is at least 10 s. i.e., if the seawater
47 temperature varies, more than 10 s is required for the carbonate species to approach equilibrium.

48 There is a temperature gradient in the thermal boundary layer (TBL), and the temperature at the top
49 of the TBL is lower than that at the bottom of the TBL due to the cool skin effect. The typical thickness
50 of the TBL (L) is 1 mm (Jähne, 2009). The mass boundary layer (MBL) is at the top of the TBL with a
51 typical thickness of 0.1 mm (Jähne, 2009). Molecular diffusion dominates water mass transport
52 within MBL. There is a viscous boundary layer (VBL) below the MBL and the VBL has a similar
53 thickness as the TBL (i.e., $L \sim 1$ mm) (Jähne, 2009). Viscous dissipation dominates water mass
54 transport in the VBL (Jähne, 2009). The kinematic viscosity (ν) is $\sim 1 \text{ mm}^2 \text{ s}^{-1}$ at 25°C seawater (ν is
55 larger at colder seawater). So, the timescale of water mixing in the TBL (below the MBL) is $\sim 1 \text{ s} (L^2 /$
56 $\nu)$.

57

58 **Text S3. SST Dataset for Air-Sea CO_2 Flux Estimates**

59 The SST data used for flux estimates differ between studies. Table S1 lists SST datasets used in eight
60 global observation-based (i.e., $f\text{CO}_2$ -based) air-sea CO_2 flux estimates. Within a specific study, the
61 same global gap-free SST dataset is typically used for the calculation of Schmidt number, Sc ,
62 solubility at the base of the MBL, α_w , and at the air-sea interface, α_i , CO_2 fugacity in the atmosphere,
63 $f\text{CO}_{2a}$, and for the $f\text{CO}_{2w}$ mapping, while the *in-situ* bulk water temperature (T_{Bulk}) measured
64 concurrently with $f\text{CO}_{2w}$ is used for correcting individual $f\text{CO}_{2w}$ from the equilibrator temperature to
65 the seawater temperature.

66 An exception to the above is Watson et al. (2020), which co-located the DOISST v2.0 ($1^\circ \times 1^\circ$, monthly
67 data) (Reynolds et al., 2007) to the individual $f\text{CO}_{2w}$ measurements in SOCAT (Goddijn-Murphy et al.,
68 2015). The co-located DOISST v2.0 was used to re-calculate $f\text{CO}_{2w}$ (via Equation 2 in the main text).
69 Watson et al. (2020) showed that SOCAT SST is on average 0.13 ± 0.78 K higher than the co-located
70 DOISST v2.0, and the SOCAT $f\text{CO}_{2w}$ is on average 1.65 ± 11.98 μatm higher than the re-calculated
71 $f\text{CO}_{2w}$. Watson et al. (2020) and this study are the only two studies that considered the cool skin effect.
72 Watson et al. (2020) applied a constant cool skin correction (0.17 K) to the satellite subskin SST
73 product (i.e., DOISST v2.0 minus 0.17 K) for the calculation of α_i and $f\text{CO}_{2a}$. In addition, Watson et al.
74 (2020) used HadISST for the mapping process instead of the SST product used to calculate the other
75 variables (i.e., DOISST v2.0).

76 As discussed in the main text, a global gap-free T_{Subskin} product is an important practical SST for the
77 air-sea CO_2 flux calculation. However, only some of the global gap-free SST products in Table S1
78 (MOISST v2, DOISST v2.0, OAFflux, and CCI SST v2.1) represent the subskin temperature, while the
79 others (ASMD, ARMOR3D, MGDSST, HadISST) correspond to the temperature of bulk seawater.

80

81 **Text S4. Comparison of Three Satellite SST Products**

82 The satellite SST product is expected to provide a consistent subskin temperature which can be used
83 for calculating global Sc , α_w , α_i , and $f\text{CO}_{2a}$, and for mapping $f\text{CO}_{2w}$. Recent research compared eight
84 global gap-free satellite/blend SST products (ESA CCI SST v2.0, ERA5, HadISST1, DOISST v2.1, MUR25
85 v4.2, MGDSST, BoM Monthly SST, OSITASST) and showed that the global mean of these eight SST
86 products ranges from 20.02 $^\circ\text{C}$ to 20.17 $^\circ\text{C}$ (for the period 2003-2018 with 95% confidence level)
87 (Yang et al., 2021). So, a bias potentially exists in some or all of these satellite SST products. In
88 addition, among these eight satellite SST products, only the CCI SST (Merchant et al., 2019; Merchant
89 & Embury, 2020) and the DOISST (Huang et al., 2021; Reynolds et al., 2007) represent the subskin
90 temperature (Yang et al., 2021). The other SST products provide a bulk temperature for a depth
91 below the subskin. So, hereafter, only the CCI SST and the OISST (DOISST and MOISST) are assessed.

92 There are two types of OISST products: 1) $1^\circ \times 1^\circ$, monthly OI.V2 SST (MOISST), which is derived by
93 linear interpolation of the $1^\circ \times 1^\circ$, weekly OI.v2 SST fields to daily fields which are then averaged
94 over a month (Reynolds et al., 2002); 2) $1/4^\circ \times 1/4^\circ$, daily OISST v2 (Reynolds et al., 2007) which has
95 been replaced by DOISST v2.1 (Huang et al., 2021) with some quality improvements for data from
96 January 1, 2016, onwards. DOISST data are constructed differently than the MOISST, although both
97 use satellite-derived SST data with a calibration based on *in-situ* measurements (including both
98 ICOADS ship and drifting buoy SST) (Freeman et al., 2017; Xu & Ignatov, 2014). With the warm bias
99 in the ICOADS ship SST well-recognized by the SST community (Huang et al., 2017; Kennedy et al.,
100 2011, 2019), a constant (0.14 K) is subtracted from the ICOADS ship SST to compensate for the large
101 scale (global mean) ship-buoy SST difference (Reynolds & Chelton, 2010) before it is used to calibrate
102 the DOISST v2.0. In addition, the latest research shows that the bias in the ICOADS ship SST has
103 substantially reduced since 2006 (Kennedy et al., 2019). So for the DOISST v2.1 dataset, the ship-
104 buoy SST difference has been set to 0.14 K from 1981 to 2015 and to 0.01 K from 2016 onwards
105 (Huang et al., 2021). However, the warm bias in the ICOADS ship SST is not corrected for when it is
106 used for the calibration of the MOISST. So the DOISST tends to be lower than the monthly MOISST,
107 particularly in the 1980s and 1990s when ship SST data were dominant (Banzon et al., 2016).

108 Here we test the agreement between the gridded drifting buoy SST (as a reference SST; Xu & Ignatov,
109 2014) and three satellite SST products: CCI SST v2.1, MOISST v2, DOISST v2.1. Figure S1a shows a
110 comparison between different SST products. The DOISST v2.1 is on average 0.09 K lower than the
111 buoy SST (red curve), while the MOISST v2 is on average 0.01 K lower than the buoy SST (blue curve).
112 The orange curve shows that the CCI SST v2.1 is on average 0.05 K lower than the buoy SST.

113 Although MOISST v2 has the smallest bias, it is an old SST product and has not been updated for a
114 long time. The standard deviation (SD) of MOISST minus the buoy SST (blue line in Figure S1b) is
115 larger than that of DOISST v2.1 (or CCI SST v2.1) minus buoy SST (red and orange lines in Figure S1b).
116 Therefore, we suggest that the MOISST should better not be used for air-sea CO₂ flux estimates.

117 The SD of DOISST v2.1 minus the buoy SST is similar to the SD of CCI SST v2.1 minus the buoy SST
118 (red and orange line in Figure S1b). Therefore, both DOISST v2.1 and CCI SST v2.1 can be used for
119 the air-sea CO₂ flux estimates (i.e., calculating global Sc , α_w , α_i , fCO_{2a} , and mapping fCO_{2w}). However,
120 as the *in-situ* SST measurements were employed for the validation process, DOISST and MOISST are
121 not fully independent from the *in-situ* SSTs. The CCI SST is independent from the *in-situ* SST dataset
122 because the CCI SST is not calibrated against *in-situ* SST measurements as a reduced-state-vector
123 optimal estimation algorithm (Merchant et al., 2019) is used instead.

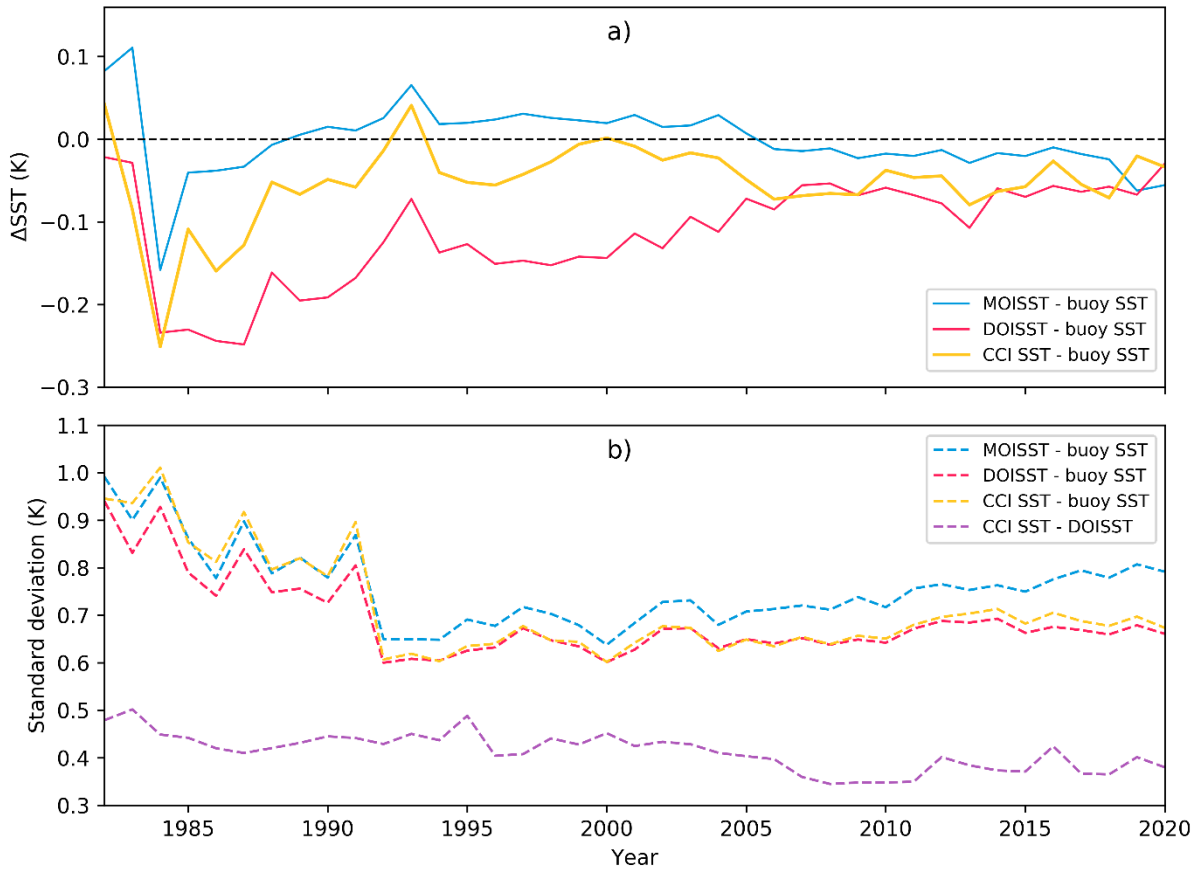
124 The purple line in Figure S1b shows that the SD of CCI SST v2.1 minus DOISST v2.1 is ~0.5 K and
125 decreasing to ~0.4 K in recent years, which suggests that there is a discrepancy between these two
126 satellite SST products. the SD of DOISST v2.0 minus SOCAT SST is ~0.8 K. The large SDs suggest that
127 using any co-located satellite SST products to calculate $f\text{CO}_{2w}$ could significantly increase the
128 uncertainty in $f\text{CO}_{2w}$ and thus the uncertainty in the estimated air-sea CO_2 flux.

129

130 **Text S5. Under-Sampling and inter-Annual Variation of the Bias Correction**

131 Due to the limited measurements in SOCAT and buoy SST datasets, especially during the 1980s,
132 many grid cells only have a small number of SOCAT and buoy SST measurements. The number of
133 measurements in grid cells might influence the comparison between the SOCAT SST and the buoy
134 SST. Figure S2a shows the under-sampling issue and its influence on the average of SOCAT SST
135 minus buoy SST. If we consider all matched grid cells, the average of SOCAT SST minus buoy SST is
136 ~0.02 K. But if we consider cells with at least 10 measurements, the average of SOCAT SST minus
137 buoy SST is ~0.03 K. However, Figure S2b suggests that under-sampling does not significantly
138 influence the latitudinal variation of SOCAT SST minus buoy SST.

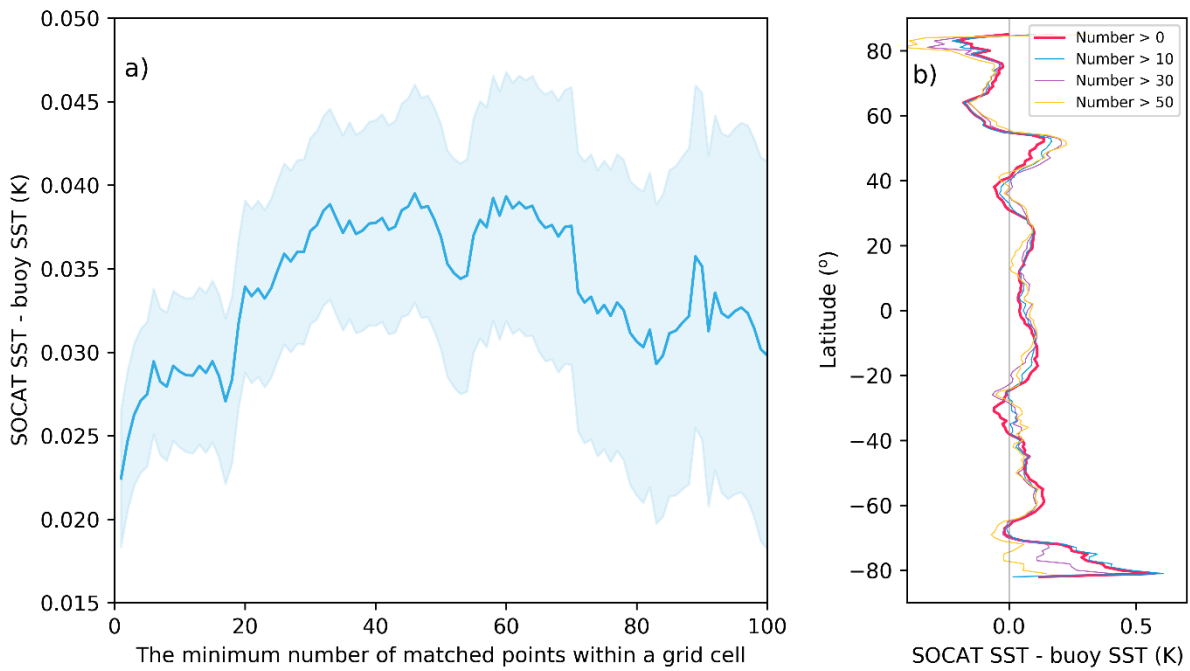
139 Figure S3 shows the inter-annual variation of the number of cells with SOCAT measurements and
140 the bias correction for the SOCAT SST. We apply the latitudinal-varying bias correction (red curve in
141 Figure S2b) to account for the bias in the SOCAT SST (use buoy SST as the reference). However, as
142 the number of SOCAT measurements varies with year, and the measurements in years before 1990
143 are limited (blue bars in Figure S3), we do not consider inter-annual variation of the latitudinal-
144 varying bias correction. Thus, the same bias correction value is applied to a specific latitude for every
145 year (every month) between 1982 and 2020. However, as the spatial distribution of the SOCAT
146 measurements is different in different years, the annual mean bias correction varies with year (red
147 line in Figure S3).



148

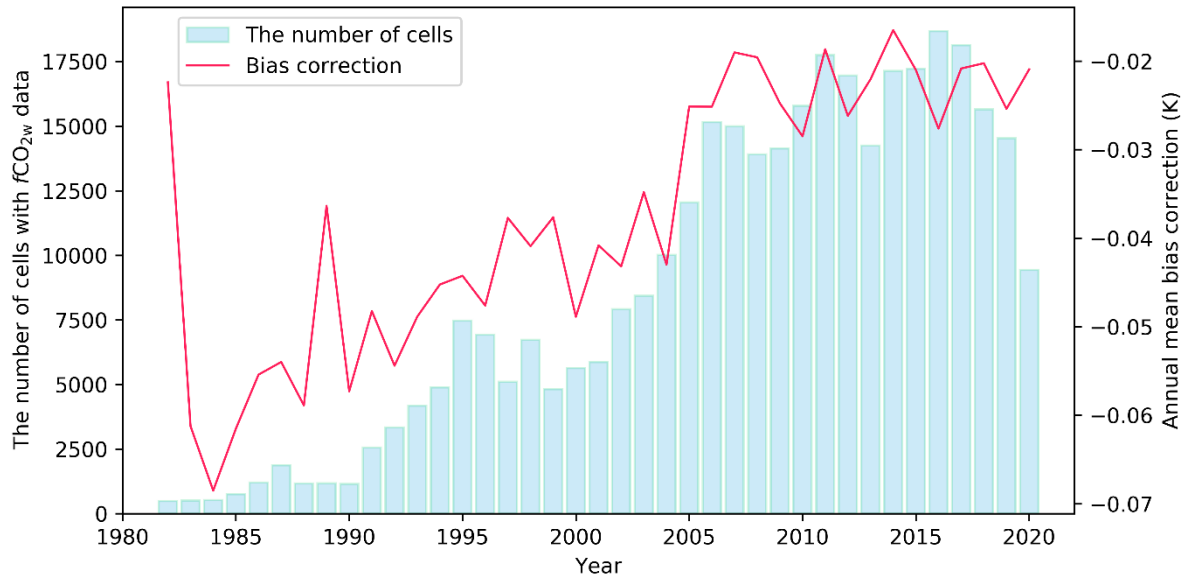
149 **Figure S1.** Time series of the global annual mean SST difference and its standard deviation between
 150 SST products. (a) The blue, red and orange lines represent the MOISST v2 (MOISST) minus drifting
 151 buoy SST, DOISST v2.1 (DOISST) minus buoy SST, and ESA CCI SST v2.1 (CCI SST) minus buoy SST,
 152 respectively. (b) The blue, red, orange, and purple dashed lines correspond to the standard deviation
 153 of MOISST minus buoy SST, DOISST minus buoy SST, CCI SST and buoy SST, and CCI SST minus
 154 DOISST, respectively.

155



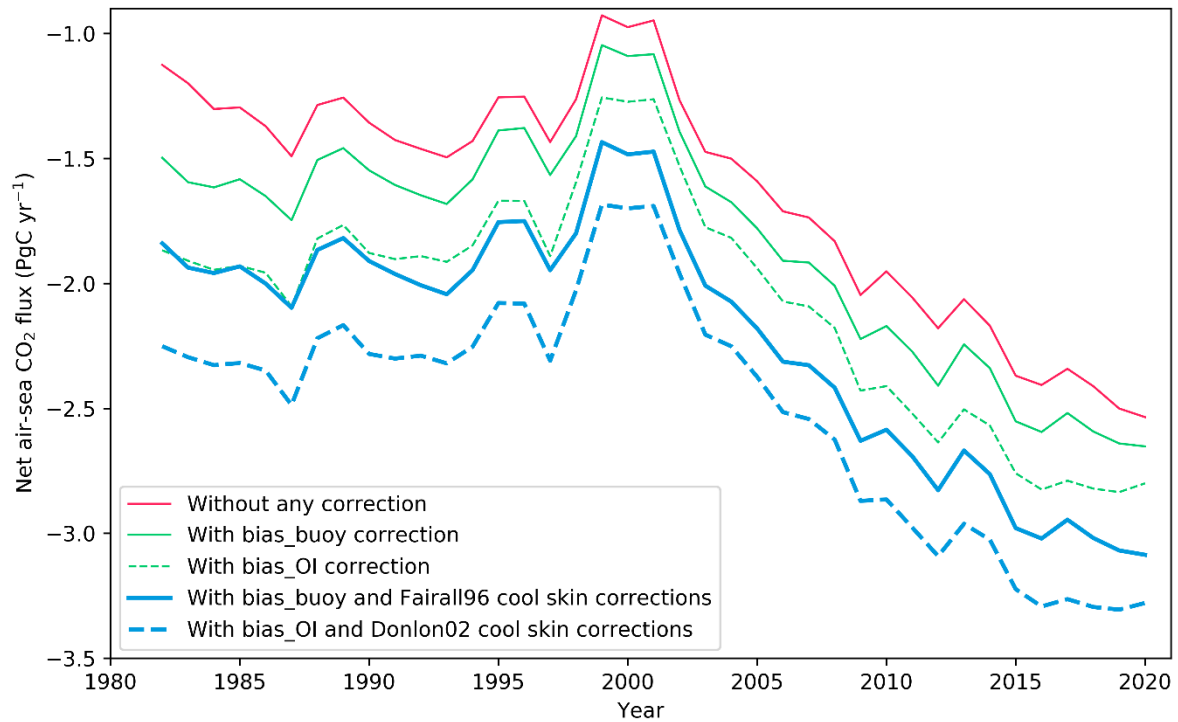
156

157 **Figure. S2.** (a) Average of SOCAT SST minus buoy SST (from 1982 to 2020) versus the minimum
 158 number of matched points within a grid cell, and (b) the latitudinal variation of SOCAT SST minus
 159 buoy SST. The first (second) point in (a) represents the average temperature difference considering
 160 all grid cells with at least one (two) SOCAT and one (two) buoy measurement (s). The blue shading
 161 indicates one standard deviation. The red, blue, purple, and orange lines in (b) correspond to the
 162 average temperature difference for grid cells with at least one, eleven, thirty one, and fifty one
 163 matched SOCAT and buoy measurements, respectively .



164

165 **Figure S3.** The number of grid cells (per year) with measurements in the $1^\circ \times 1^\circ$, monthly gridded
 166 SOCAT data (blue bars) and the inter-annual mean bias correction for the SOCAT SST (red line)
 167 assessed by the buoy SST.



168

169 **Figure S4.** Time series of the annual mean global net air-sea CO₂ flux calculated by interpolating the
 170 sea surface CO₂ fugacity ($f\text{CO}_{2w}$) data in SOCATv2021 using a neural network-based method
 171 (Landschützer et al., 2013). Negative values represent ocean CO₂ uptake. The red, green, and blue
 172 solid lines represent the uncorrected flux, the flux with bias_buoy correction (bias assessed by buoy
 173 SST), and the flux with bias_buoy and Fairall96 cool skin corrections, respectively (this study). The
 174 green and blue dashed curves correspond to the flux with the bias_OI (using co-located DOISST v2.1
 175 to account for the bias in SOCAT SST) and Donlon02 cool skin corrections (Watson et al., 2020). The
 176 same datasets, interpolation method (Landschützer et al., 2013), and the Arctic and the coastal flux
 177 compensation method (Fay et al., 2021) are used for the flux calculations in the figure.

178

179 **Table S1.** Summary of the SST datasets used in global air-sea CO₂ flux estimates by the bulk flux
 180 method (Equation 1 in the main text). Acronyms of SST products and related references are in the
 181 footnotes.

| Studies | Sc and α_w | α_i and $f\text{CO}_{2a}$ | Individual $f\text{CO}_{2w}$ | $f\text{CO}_{2w}$ mapping |
|--|-------------------------------------|---|--|---|
| Takahashi et al. (2009) | ASMD | ASMD | <i>In-situ</i> T_{Bulk} | Interpolated T_{Bulk} |
| Rödenbeck et al. (2013) | OAFflux | OAFflux | <i>In-situ</i> T_{Bulk} | OAFflux |
| Zeng et al. (2014) and Landschützer et al. (2016) | MOISST v2 | MOISST v2 | <i>In-situ</i> T_{Bulk} | MOISST v2 |
| Denvil-Sommer et al. (2019) | ARMOR3D | ARMOR3D | <i>In-situ</i> T_{Bulk} | ARMOR3D |
| Gregor et al. (2019) | DOISST v2.0 | DOISST v2.0 | <i>In-situ</i> T_{Bulk} | DOISST v2.0 |
| Watson et al. (2020) | DOISST v2.0 | DOISST v2.0 – 0.17 K | Co-located DOISST v2.0 | HadISST |
| Iida et al. (2021) | MGDSST | MGDSST | <i>In-situ</i> T_{Bulk} | MGDSST |
| This study | CCI SST v2.1 | CCI SST v2.1 with a Fairall96 cool skin correction | <i>In-situ</i> T_{Bulk} with a bias correction assessed by buoy SST | CCI SST v2.1 |

182 ASMD: surface water temperature from the NOAA Atlas of Surface Marine Data (1994, as cited in
 183 Takahashi et al., 2009). OAFflux: SST from the Objectively Analysed Air-Sea Fluxes for the global
 184 oceans dataset (Yu & Weller, 2007). MOISST v2: NOAA Monthly Optimum Interpolation SST dataset
 185 version 2, also known as OI.V2 SST (Reynolds et al., 2002). ARMOR3D: SST from monthly global
 186 reprocessed products of physical variables from the ARMOR3D L4 dataset (Guinehut et al., 2012).
 187 DOISST v2.0: NOAA Daily Optimum Interpolation SST dataset version 2 (Banzon et al., 2016; Reynolds
 188 et al., 2007). HadISST: Hadley Centre Sea Ice and Sea Surface Temperature dataset (Rayner et al.,
 189 2003). MGDSST: Merged satellite and *in-situ* data global daily SST analysis dataset (Sakurai et al.,
 190 2005). CCI SST v2.1: European Space Agency Climate Change Initiative SST product (Merchant et al.,
 191 2019; Merchant & Embury, 2020). *In-situ* T_{Bulk} represents the *in-situ* bulk SST measurements in the
 192 LDEO and SOCAT datasets. The study of Takahashi et al. (Takahashi et al., 2009) used the LDEO
 193 (Lamont-Doherty Earth Observatory) $f\text{CO}_{2w}$ dataset (Takahashi et al., 2008) while the other studies
 194 employed the SOCAT $f\text{CO}_{2w}$ dataset (Bakker et al., 2016). Co-located DOISST v2.0: the $0.25^\circ \times 0.25^\circ$,
 195 daily DOISST v2.0 is resampled to $1^\circ \times 1^\circ$, monthly data and then co-located with the individual
 196 $f\text{CO}_{2w}$ measurements in SOCAT (Goddijn-Murphy et al., 2015).

197

198 **Dataset S1 (Separate file: Flux corrections with different methods. xlsx)**: Air-sea CO₂ flux
199 corrections using different methods. Lines 2–5 represent the flux corrections for different years
200 using bias_buoy, bias_OI, Fairall96, and Donlon02 temperature corrections, respectively. Lines 7–10
201 correspond to the flux corrections for different latitude bins using bias_buoy, bias_OI, Fairall96, and
202 Donlon02 temperature corrections, respectively. For example, latitude -89.5 represent the median
203 latitude of the latitude bin [-90, -89] and the corresponding flux correction represent the
204 accumulated flux in this latitude bin.

205

206

207 **SI References**

208

209 Bakker, D. C. E., Bange, H. W., Gruber, N., Johannessen, T., Upstill-Goddard, R. C., Borges, A. V, et al.
210 (2014). Air-sea interactions of natural long-lived greenhouse gases (CO₂, N₂O, CH₄) in a
211 changing climate. In P. S. Liss & M. T. Johnson (Eds.), *Ocean-atmosphere interactions of gases and*
212 *particles* (pp. 113–169). Berlin, Heidelberg: Springer Berlin Heidelberg.
213 https://doi.org/10.1007/978-3-642-25643-1_3

214 Bakker, D. C. E., Pfeil, B., Landa, C. S., Metzl, N., O'Brien, K. M., Olsen, A., et al. (2016). A multi-decade
215 record of high-quality *f*CO₂ data in version 3 of the Surface Ocean CO₂ Atlas (SOCAT). *Earth*
216 *System Science Data*, 8(2), 383–413. <https://doi.org/10.5194/essd-8-383-2016>

217 Banzon, V., Smith, T. M., Mike Chin, T., Liu, C., & Hankins, W. (2016). A long-term record of blended
218 satellite and in situ sea-surface temperature for climate monitoring, modeling and
219 environmental studies. *Earth System Science Data*, 8(1), 165–176. [https://doi.org/10.5194/essd-](https://doi.org/10.5194/essd-8-165-2016)
220 [8-165-2016](https://doi.org/10.5194/essd-8-165-2016)

221 Denvil-Sommer, A., Gehlen, M., Vrac, M., & Mejia, C. (2019). LSCE-FFNN-v1: a two-step neural network
222 model for the reconstruction of surface ocean *p*CO₂ over the global ocean. *Geoscientific Model*
223 *Development*, 12(5), 2091–2105. <https://doi.org/10.5194/gmd-12-2091-2019>

224 Fay, A. R., Gregor, L., Landschützer, P., McKinley, G. A., Gruber, N., Gehlen, M., et al. (2021). SeaFlux:
225 Harmonization of air-sea CO₂ fluxes from surface *p*CO₂ data products using a standardized
226 approach. *Earth System Science Data*, 13(10), 4693–4710. [https://doi.org/10.5194/essd-13-](https://doi.org/10.5194/essd-13-4693-2021)
227 [4693-2021](https://doi.org/10.5194/essd-13-4693-2021)

228 Freeman, E., Woodruff, S. D., Worley, S. J., Lubker, S. J., Kent, E. C., Angel, W. E., et al. (2017). ICOADS
229 Release 3.0: a major update to the historical marine climate record. *International Journal of*

230 *Climatology*, 37(5), 2211–2232. <https://doi.org/10.1002/joc.4775>

231 Goddijn-Murphy, L. M., Woolf, D. K., Land, P. E., Shutler, J. D., & Donlon, C. (2015). The OceanFlux
232 Greenhouse Gases methodology for deriving a sea surface climatology of CO₂ fugacity in
233 support of air-sea gas flux studies. *Ocean Science*, 11(4), 519–541. [https://doi.org/10.5194/os-](https://doi.org/10.5194/os-11-519-2015)
234 [11-519-2015](https://doi.org/10.5194/os-11-519-2015)

235 Gregor, L., Lebehot, A. D., Kok, S., & Scheel Monteiro, P. M. (2019). A comparative assessment of the
236 uncertainties of global surface ocean CO₂ estimates using a machine-learning ensemble (CSIR-
237 ML6 version 2019a)-Have we hit the wall? *Geoscientific Model Development*, 12(12), 5113–5136.
238 <https://doi.org/10.5194/gmd-12-5113-2019>

239 Guinehut, S., Dhomps, A. L., Larnicol, G., & Le Traon, P. Y. (2012). High resolution 3-D temperature
240 and salinity fields derived from in situ and satellite observations. *Ocean Science*, 8(5), 845–857.
241 <https://doi.org/10.5194/os-8-845-2012>

242 Huang, B., Thorne, P. W., Banzon, V. F., Boyer, T., Chepurin, G., Lawrimore, J. H., et al. (2017). Extended
243 reconstructed sea surface temperature, version 5 (ERSSTv5): Upgrades, validations, and
244 intercomparisons. *Journal of Climate*, 30(20), 8179–8205. [https://doi.org/10.1175/JCLI-D-16-](https://doi.org/10.1175/JCLI-D-16-0836.1)
245 [0836.1](https://doi.org/10.1175/JCLI-D-16-0836.1)

246 Huang, B., Liu, C., Banzon, V., Freeman, E., Graham, G., Hankins, B., et al. (2021). Improvements of the
247 daily optimum interpolation sea surface temperature (DOISST) version 2.1. *Journal of Climate*,
248 34(8), 2923–2939. <https://doi.org/10.1175/JCLI-D-20-0166.1>

249 Iida, Y., Takatani, Y., Kojima, A., & Ishii, M. (2021). Global trends of ocean CO₂ sink and ocean
250 acidification: an observation-based reconstruction of surface ocean inorganic carbon variables.
251 *Journal of Oceanography*, 77(2), 323–358. <https://doi.org/10.1007/s10872-020-00571-5>

252 Jähne, B. (2009). Air-sea gas exchange. *Elements of Physical Oceanography: A Derivative of the*
253 *Encyclopedia of Ocean Sciences*, 160–169. [https://doi.org/10.1016/B978-0-12-409548-9.11613-](https://doi.org/10.1016/B978-0-12-409548-9.11613-6)
254 [6](https://doi.org/10.1016/B978-0-12-409548-9.11613-6)

255 Johnson, K. S. (1982). Carbon dioxide hydration and dehydration kinetics in seawater. *Limnology and*
256 *Oceanography*, 27(5), 849–855. <https://doi.org/10.4319/lo.1982.27.5.0849>

257 Kennedy, J. J., Rayner, N. A., Smith, R. O., Parker, D. E., & Saunby, M. (2011). Reassessing biases and
258 other uncertainties in sea surface temperature observations measured in situ since 1850: 2.
259 Biases and homogenization. *Journal of Geophysical Research*, 116(D14), 1–22.
260 <https://doi.org/10.1029/2010jd015220>

261 Kennedy, J. J., Rayner, N. A., Atkinson, C. P., & Killick, R. E. (2019). An ensemble data set of sea surface

262 temperature change from 1850: The Met Office Hadley Centre HadSST.4.0.0.0 data set. *Journal*
263 *of Geophysical Research: Atmospheres*, 124(14), 7719–7763.
264 <https://doi.org/10.1029/2018JD029867>

265 Landschützer, P., Gruber, N., Bakker, D. C. E., Schuster, U., Nakaoka, S., Payne, M. R., et al. (2013). A
266 neural network-based estimate of the seasonal to inter-annual variability of the Atlantic Ocean
267 carbon sink. *Biogeosciences*, 10(11), 7793–7815. <https://doi.org/10.5194/bg-10-7793-2013>

268 Landschützer, P., Gruber, N., & Bakker, D. C. E. (2016). Decadal variations and trends of the global
269 ocean carbon sink. *Global Biogeochemical Cycles*, 30(10), 1396–1417.
270 <https://doi.org/10.1002/2015GB005359>

271 Merchant, C. J., & Embury, O. (2020). Adjusting for desert-dust-related biases in a climate data record
272 of sea surface temperature. *Remote Sensing*, 12(16), 1–15. <https://doi.org/10.3390/RS12162554>

273 Merchant, C. J., Embury, O., Bulgin, C. E., Block, T., Corlett, G. K., Fiedler, E., et al. (2019). Satellite-based
274 time-series of sea-surface temperature since 1981 for climate applications. *Scientific Data*, 6(1),
275 1–18. <https://doi.org/10.1038/s41597-019-0236-x>

276 Pierrot, D., Neill, C., Sullivan, K., Castle, R., Wanninkhof, R., Lüger, H., et al. (2009). Recommendations
277 for autonomous underway $p\text{CO}_2$ measuring systems and data-reduction routines. *Deep-Sea*
278 *Research Part II: Topical Studies in Oceanography*, 56(8–10), 512–522.
279 <https://doi.org/10.1016/j.dsr2.2008.12.005>

280 Rayner, N. A., Parker, D. E., Horton, E. B., Folland, C. K., Alexander, L. V., Rowell, D. P., et al. (2003).
281 Global analyses of sea surface temperature, sea ice, and night marine air temperature since the
282 late nineteenth century. *Journal of Geophysical Research: Atmospheres*, 108(14).
283 <https://doi.org/10.1029/2002jd002670>

284 Reynolds, R. W., & Chelton, D. B. (2010). Comparisons of daily Sea surface temperature analyses for
285 2007–08. *Journal of Climate*, 23(13), 3545–3562. <https://doi.org/10.1175/2010JCLI3294.1>

286 Reynolds, R. W., Rayner, N. A., Smith, T. M., Stokes, D. C., & Wang, W. (2002). An improved in situ and
287 satellite SST analysis for climate. *Journal of Climate*, 15(13), 1609–1625.
288 [https://doi.org/10.1175/1520-0442\(2002\)015<1609:AIISAS>2.0.CO;2](https://doi.org/10.1175/1520-0442(2002)015<1609:AIISAS>2.0.CO;2)

289 Reynolds, R. W., Smith, T. M., Liu, C., Chelton, D. B., Casey, K. S., & Schlax, M. G. (2007). Daily high-
290 resolution-blended analyses for sea surface temperature. *Journal of Climate*, 20(22), 5473–5496.
291 <https://doi.org/10.1175/2007JCLI1824.1>

292 Rödenbeck, C., Keeling, R. F., Bakker, D. C. E., Metzl, N., Olsen, A., Sabine, C., & Heimann, M. (2013).
293 Global surface-ocean $p\text{CO}_2$ and sea-Air CO_2 flux variability from an observation-driven ocean

294 mixed-layer scheme. *Ocean Science*, 9(2), 193–216. <https://doi.org/10.5194/os-9-193-2013>

295 Sakurai, T., Yukio, K., & Kuragano, T. (2005). Merged satellite and in-situ data global daily SST. In
296 *Proceedings. 2005 IEEE International Geoscience and Remote Sensing Symposium, 2005. IGARSS'05.*
297 (Vol. 4, pp. 2606–2608). IEEE.

298 Takahashi, T., Sutherland, S. C., & Kozyr, A. (2008). Global ocean surface water partial pressure of CO₂
299 database: Measurements performed during 1968–2006 (Version 1.0). *ORNL/CDIAC-152, NDP-*
300 *088. Carbon Dioxide Information Analysis Center, Oak Ridge National Laboratory, US Department*
301 *of Energy, Oak Ridge, TN, 37831, 20.*

302 Takahashi, T., Sutherland, S. C., Wanninkhof, R., Sweeney, C., Feely, R. A., Chipman, D. W., et al. (2009).
303 Climatological mean and decadal change in surface ocean pCO₂, and net sea-air CO₂ flux over
304 the global oceans. *Deep Sea Research Part II: Topical Studies in Oceanography*, 56(8–10), 554–577.
305 <https://doi.org/10.1016/J.DSR2.2008.12.009>

306 Watson, A. J., Schuster, U., Shutler, J. D., Holding, T., Ashton, I. G. C., Landschützer, P., et al. (2020).
307 Revised estimates of ocean-atmosphere CO₂ flux are consistent with ocean carbon inventory.
308 *Nature Communications*, 11(1), 1–6. <https://doi.org/10.1038/s41467-020-18203-3>

309 Weiss, R. F. (1974). Carbon dioxide in water and seawater: the solubility of a non-ideal gas. *Marine*
310 *Chemistry*, 2(3), 203–215. [https://doi.org/10.1016/0304-4203\(74\)90015-2](https://doi.org/10.1016/0304-4203(74)90015-2)

311 Xu, F., & Ignatov, A. (2014). In situ SST quality monitor (i Quam). *Journal of Atmospheric and Oceanic*
312 *Technology*, 31(1), 164–180. <https://doi.org/10.1175/JTECH-D-13-00121.1>

313 Yang, C., Leonelli, F. E., Marullo, S., Artale, V., Beggs, H., Nardelli, B. B., et al. (2021). Sea surface
314 temperature intercomparison in the framework of the copernicus climate change service (C3S).
315 *Journal of Climate*, 34(13), 5257–5283. <https://doi.org/10.1175/JCLI-D-20-0793.1>

316 Yu, L., & Weller, R. A. (2007). Objectively analyzed air–sea heat fluxes for the global ice-free oceans
317 (1981–2005). *Bulletin of the American Meteorological Society*, 88(4), 527–540.
318 <https://doi.org/10.1175/BAMS-88-4-527>

319 Zeebe, R. E., & Wolf-Gladrow, D. (2001). *CO₂ in seawater: equilibrium, kinetics, isotopes*. Elsevier Science,
320 pp. 85–140.

321 Zeng, J., Nojiri, Y., Landschützer, P., Telszewski, M., & Nakaoka, S. (2014). A global surface ocean fCO₂
322 climatology based on a feed-forward neural network. *Journal of Atmospheric and Oceanic*
323 *Technology*, 31(8), 1838–1849. <https://doi.org/10.1175/JTECH-D-13-00137.1>

324